https://doi.org/10.5194/egusphere-2023-634
Preprint. Discussion started: 11 April 2023

On the importance to consider the cloud dependence in parameterizing the albedo of snow on sea ice

Lara Foth[1], Wolfgang Dorn[1], Annette Rinke[1], Evelyn Jäkel[2], and Hannah Niehaus[3]

[1]Alfred Wegener Institute, Helmholtz Centre for Polar and Marine Research, Potsdam, Germany
[2]Leipzig Institute for Meteorology, University of Leipzig, Leipzig, Germany
[3]Institute of Environmental Physics, University of Bremen, Bremen, Germany

Correspondence: Wolfgang Dorn (wolfgang.dorn@awi.de)

Abstract. The impact of a revised snow surface albedo parameterization, which explicitly considers the cloud dependence of the snow albedo, is evaluated in simulations of a coupled regional climate model of the Arctic. The revised snow surface albedo parameterization leads to a more realistic simulation of the variability of the surface albedo during the snow melt period in late May and June. In particular, the reproduction of lower albedo values under cloud-free/broken-cloud conditions during the snow melt period represents a major improvement and results in an earlier disappearance of the snow cover and an earlier onset of sea-ice melt. In this way, the consideration of the cloud dependence of the snow albedo results in an amplification of the two-stage snow-albedo/ice-albedo feedback in the model. This finds expression in additional loss of sea-ice volume of more than 1000 km^3 and additional reduction of summer sea-ice extent of around 250,000 km^2 during one melting period, with accumulating magnitude of the overall changes in subsequent years.

1 Introduction

The surface albedo feedback effect is one of the main contributors to Arctic amplification (e.g., Pithan and Mauritsen, 2014; Hahn et al., 2021). It is known that "cloud cover normally causes an increase in spectrally integrated snow albedo" (Warren, 1982). Sensitivity studies already showed that "the increase in surface albedo with cloud cover can cause a doubling of the ice thickness" in model simulations (Shine and Henderson-Sellers, 1985). A couple of modeling studies addressed the importance of improving the sea-ice albedo parameterization (e.g., Liu et al., 2007; Toyoda et al., 2020); however, the cloud dependence of the surface albedo has not been considered explicitely in corresponding climate simulations by using appropriate parameterizations.

The cloud dependence of the surface albedo was demonstrated in several studies (Grenfell and Perovich, 2008; Gardner and Sharp, 2010; Stapf et al., 2020). It is caused by the different spectral characteristics of the incident radiation in a cloudy atmosphere (spectrally almost neutral) compared to cloudless conditions (strong spectral slope) and multiple surface–cloud interactions over highly reflecting surfaces. In the presence of clouds, the transmitted downward irradiance is weighted to shorter (visible) wavelengths, causing an increase in shortwave surface albedo, in particular in the polar regions where the solar zenith angle is large. This process seems to outweigh the albedo decreasing effect of a shift from mainly direct to rather

https://doi.org/10.5194/egusphere-2023-634
Preprint. Discussion started: 11 April 2023

Table 1. Albedo values for cold, dry snow (α_{dry}, for $T \leq T_{\mathrm{dry}}$) and warm, wet snow (α_{wet}, for $T = 0\,^{\circ}\mathrm{C}$) and temperature threshold (T_{dry}) in the original and the revised snow albedo parameterization. The revised snow albedo parameterization distinguishes between overcast conditions (cloud cover $\geq 95\,\%$) and cloud-free/broken-cloud conditions (cloud cover $< 95\,\%$). For temperatures $T_{\mathrm{dry}} < T < 0\,^{\circ}\mathrm{C}$ a linear transition between α_{dry} and α_{wet} is applied.

parameterization	clouds	α_{dry}	α_{wet}	T_{dry} (°C)
original	–	0.84	0.77	−0.01
revised	overcast	0.88	0.80	−3.0
revised	non-overcast	0.79	0.66	−2.5

diffuse irradiance in cloudy conditions, which decreases the surface albedo. Nonetheless, only few coupled climate models consider the cloud dependence in their surface albedo parameterization (e.g., Boucher et al., 2020; Döscher et al., 2022).

Although the sea-ice surface can consist of dry snow, melting snow, bare and melting ice, melting and refreezing ponded ice, and sediment-laden ice (Light et al., 2022), we focus for now on the parameterization of the snow albedo. We use a coupled regional climate model for the Arctic in order to demonstrate the importance of a cloud-cover-dependent snow albedo parameterization for the sea-ice evolution in coupled climate model simulations. This revised snow albedo parameterization was suggested by Jäkel et al. (2019) on the basis of broadband surface albedo measurements carried out north of Svalbard in May/June 2017. Compared to the original parameterization by Køltzow (2007), it includes different values for dry and wet snow and a modified temperature threshold, at which the snow is considered as dry, but it additionally distinguishes between overcast conditions and non-overcast conditions (see Table 1).

The performance of the revised snow albedo parameterization is compared with the original parameterization by Køltzow (2007) and evaluated against irradiance and cloud cover observations. Finally, the impact of considering a cloud-cover-dependent snow albedo parameterization on the modeled sea-ice evolution is demonstrated.

2 Data

2.1 Model simulations

Two simulations, which only differ in the snow albedo parameterization, were carried out with the coupled regional climate model HIRHAM–NAOSIM (Dorn et al., 2019). One simulation used the original snow albedo parameterization by Køltzow (2007) (hereinafter referred to as HNold), while the other used the revised snow albedo parameterization by Jäkel et al. (2019) (hereinafter referred to as HNnew). HIRHAM–NAOSIM is applied over a circum-Arctic domain using rotated latitude-longitude grids with horizontal resolution of 1/4° (∼ 27 km) in the atmosphere component HIRHAM and 1/12° (∼ 9 km) in the ocean–sea ice component NAOSIM. More detailed information on the model components and their coupling is given by Dorn et al. (2019). The full details about the model's sea-ice albedo parameterization are described by Dorn et al. (2009), and information on the model's cloud parameterization is given by Klaus et al. (2016).

https://doi.org/10.5194/egusphere-2023-634
Preprint. Discussion started: 11 April 2023

The simulations were carried out for the period 2019–2020, driven by ERA5 reanalysis data (Hersbach et al., 2020) at HIRHAM's lateral boundaries as well as HIRHAM's lower and NAOSIM's upper boundaries, which lie outside the coupling domain (defined as the overlap area of the components' model domains). For NAOSIM's open lateral boundaries, ORAS5 reanalysis data (Zuo et al., 2019) were used. HIRHAM's prognostic fields, consisting of surface air pressure, horizontal wind components, air temperature, specific humidity, cloud liquid water content, and cloud ice content, were nudged to the corresponding ERA5 fields with a vertically uniform nudging time scale of 16.67 h (which corresponds to a nudging of 1 % per time step) in order to reproduce the observed synopic and large-scale atmospheric conditions.

2.2 Observations

For the evaluation of the two snow albedo parameterizations, observational data from the Multidisciplinary drifting Observatory for the Study of Arctic Climate (MOSAiC) expedition (Shupe et al., 2022) were used. For the calculation of the surface albedo, irradiance measurements from an attended radiation station at MOSAiC's Met City location in the "Central Observatory" (MetCity) and from two autonomous atmospheric surface flux stations (ASFS30, ASFS50) that were deployed at different locations across the MOSAiC network were used. The irradiance measurements were carried out with upward and downward facing secondary-standard pyranometers; at Met City these were aspirated Eppley PSPs while at the ASFS these were internally-aspirated Hukseflux SR30-D1 pyranometers. More detailed information on the measurements are given by Cox et al. (2023). The calculation of the surface albedo from irradiance measurements at the atmospheric surface flux stations, particularly from ASFS30, was necessary, since the regular albedo measurements at Met City were suspended from 12 May to 17 June 2020 due to the transition of the research vessel *Polarstern* (Light et al., 2022); during this period ASFS30 was installed nearby the Met City location.

In addition, the surface albedo derived with the Melt Pond Detection (MPD) algorithm (Zege et al., 2015; Istomina et al., 2015b, a) from optical satellite observations (OLCI) were used for comparison. The data are produced as daily averages and gridded to a polar stereographic grid at a resolution of 6.25 km using the spectral-to-broadband conversion method described by Pohl et al. (2020). It is important to note that these optical measurements are limited to cloud-free conditions.

For cloud cover fraction, data from the ShupeTurner cloud microphysics product (Shupe, 2022) were used.

For consistency with the three-hourly model output, equivalent three-hourly means were calculated from all measurement data used in this study, except the OLCI data. For the OLCI albedo product, daily values were calculated by averaging all data points that fall within a single model grid cell. To compare model and observation, always data from the nearest model grid cell to the atmospheric surface flux station ASFS30 were selected. Model data for times without observational data were not taken into account.

3 Results

Since this study focuses on the snow surface albedo, the analysis is restricted to the period where the incident solar radiation is relevant and where the sea-ice surface is almost entirely (> 98 %) covered by snow in the two model simulations. This

https://doi.org/10.5194/egusphere-2023-634
Preprint. Discussion started: 11 April 2023

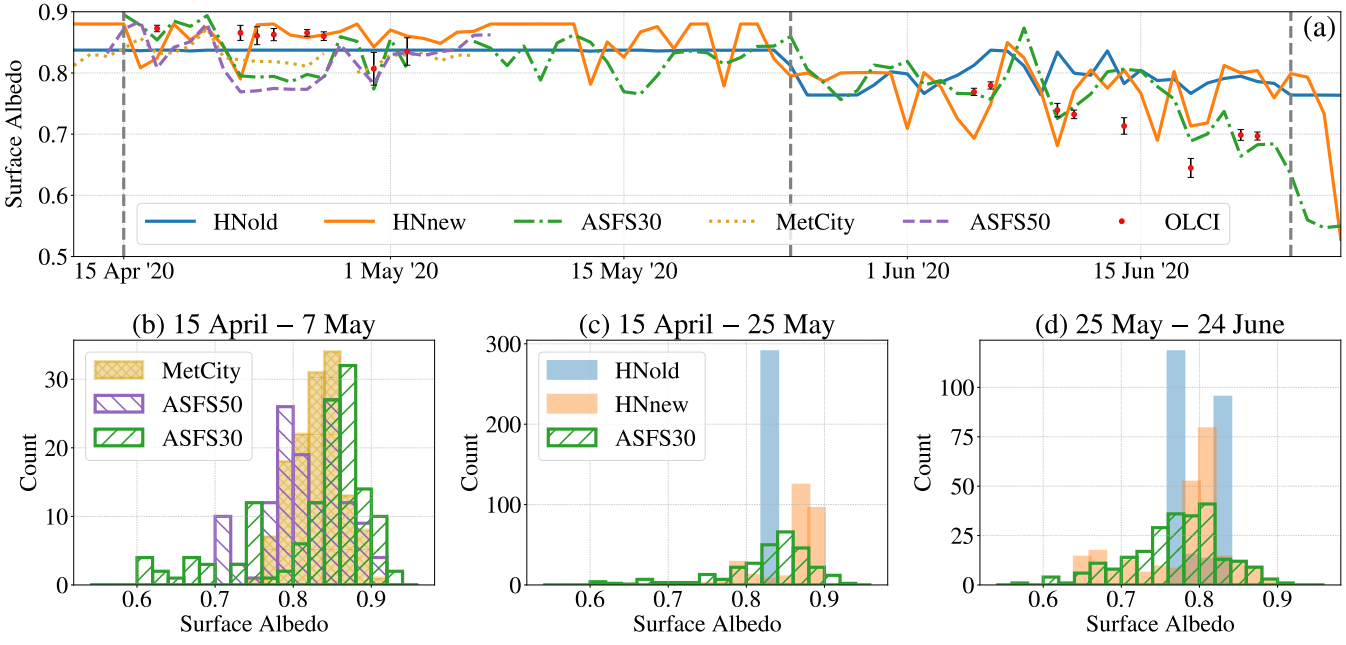

Figure 1. Top: (a) Time series of daily mean sea-ice surface albedo from the two simulations (HNold and HNnew), from three irradiance measurements (ASFS30, MetCity, ASFS50), and from the satellite observations (OLCI) for the period from mid-April 2020 to end of June 2020. The dashed vertical lines indicate the beginning and the end, respectively, of the two evaluation periods, the cold period (15 April–25 May) and the snow melt period (25 May–24 June). Bottom: Frequency distribution of three-hourly mean sea-ice surface albedo from (b) the three irradiance measurements for the period where measurements from all three sites are available, (c) the two simulations and ASFS30 for the cold period, and (d) the two simulations and ASFS30 for the snow melt period.

period starts in mid-April and ends on 24 June 2020. It is further subdivided into an early cold period (15 April–25 May), with temperatures almost exclusively below T_{dry}, and a late warmer period (25 May–24 June), with temperatures at or near the freezing point, where the snow begins to melt.

During the cold period, the sea-ice surface albedo in HNold is almost entirely defined by the albedo of dry snow without any variation (Figs. 1a and 1c). In contrast, the measurements from all three sites show distinct variations of the daily mean albedo (Fig. 1a) and even a broad spectrum of surface albedo values on a three-hourly basis (Fig. 1b). Although the measured albedo variations might not solely be attributable to changes in cloud cover, but also to local changes in the surface characteristics at the measurement site, which a climate model can not capture, it is obvious that a constant albedo in models is far from reality.

Since HNnew shows albedo variations, even if they are less pronounced than in the measurements (Figs. 1a and 1c), the implementation of a cloud dependence may be considered as one step into the right direction. Nevertheless, the values chosen for the albedo of cold, dry snow in HNnew, particularly for overcast conditions, appear to be too high as compared to the measurements. Even when considering that the three individual measurements depend on the local conditions at the measurement

https://doi.org/10.5194/egusphere-2023-634
Preprint. Discussion started: 11 April 2023

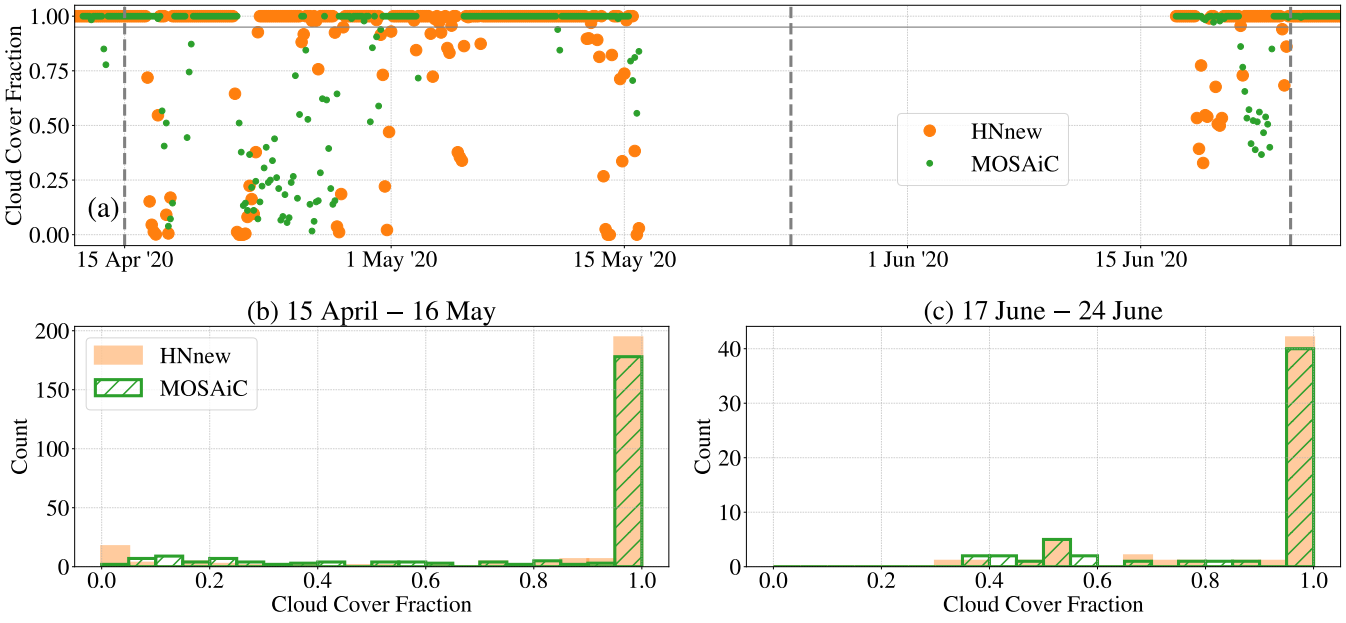

Figure 2. Top: (a) Time series of three-hourly mean total cloud cover fraction from the simulation HNnew and the MOSAiC measurements for the period from mid-April 2020 to end of June 2020. The dashed vertical lines indicate the beginning and the end, respectively, of the two evaluation periods, the cold period (15 April–25 May) and the snow melt period (25 May–24 June). Bottom: Frequency distribution of three-hourly mean total cloud cover fraction from the simulation HNnew and the MOSAiC measurements for (b) the cold period and (c) the snow melt period. MOSAiC measurements are not available between 16 May and 17 June due to the transition of the research vessel *Polarstern*.

site, which might not be representative of the model's grid-cell area, the dry-snow albedo in HNnew is mostly higher than in the measurements.

In the cold period, overlapping OLCI albedo data are only available between mid-April and beginning of May, rather agreeing with the HNnew albedo than with the three pyranometer point measurements. However, the high albedo values in HNnew indicate overcast conditions, while the OLCI albedo always indicates cloud-free conditions. Interestingly, the variance of the satellite albedo increases (30 April and 2 May) where the point measurements become more similar. This might be caused by the spatial resolution closer to that of the model, not capturing the surface heterogeneity. In the snow melt period, the OLCI albedo shows a progressive reduction with slight fluctuations that exceed the negative albedo trend of the two model runs. Nevertheless, the satellite albedo basically agrees with the point measurements, except for 14 June and 18 June where the satellite albedo is considerably lower than the albedo from the point measurements.

During the snow melt period, HNold shows two distinct maxima of the sea-ice surface albedo, which relate to the albedo values of wet snow and dry snow (Fig. 1d). Values in between appear very seldom due to the small difference between T_{dry} and the freezing point. Albedo variations in HNold are solely a result of temperature fluctuations and do not reflect the large variations that appear in the measurements.

https://doi.org/10.5194/egusphere-2023-634
Preprint. Discussion started: 11 April 2023

In comparison to HNold, the sea-ice surface albedo in HNnew shows a broad spectrum of albedo values in the range of 0.66 and 0.88 with a maximum between the two maxima of HNold. This spectrum is almost as broad as in the measurements, and also the mean values (0.78 vs. 0.77) and the standard deviations (0.06 each) statistically agree at the 95 % confidence level. In particular, albedo values below 0.74, which can not occur in HNold, appear with similar frequency as in the measurements and indicate wet or partly wet snow under cloud-free/broken-cloud conditions. Since the amount of solar radiation that reaches the surface is generally larger under non-overcast than under overcast conditions, this feature promotes the melting of the snow cover.

In both periods, non-overcast conditions (here defined as total cloud cover fraction less than 95 %) appear in HNnew only in less than one third of all cases (Figs. 2b and 2c), with a few cloud-free cases in the cold period and absolutely no cloud-free cases, but a couple of broken-cloud cases in the snow melt period. Although the simulation of clouds is generally regarded as one of the largest uncertainties in climate models (Flato et al., 2013), the cloud cover distribution in HNnew statistically agrees with the MOSAiC measurements in terms of mean value and standard deviation. Despite this statistical agreement, overcast and non-overcast conditions do not always appear at the same time (Fig. 2a). Consequently, the cloud-cover-dependent snow albedo can only statistically agree with the measurements. Nevertheless, the correspondence between the occurrence of cloud-free/broken-cloud conditions and the decrease in albedo is evident in both the HNnew simulation and the observations.

Even though cloud-free/broken-cloud conditions appear not very often in HNnew, the intermittently occurring lower albedo values during the snow melt period amplify the melting of the snow. This is reflected in the fact that the residual atmospheric heat flux Q_{res} available for melting of snow and sea ice is on average 3.6 W m^{-2} higher in HNnew between 25 May and 24 June, with the consequence that HNnew simulates an earlier disappearance of the snow cover of roughly one week compared to HNold (not shown here). Once the snow cover has disappeared, the surplus of solar radiation during the polar day is used to melt the sea ice, often by forming melt ponds on top of the ice, whereby the surface albedo decreases further. As a result, the ice melt starts not only earlier, but also the melt rate increases due to the decrease of the albedo during a time of high solar irradiance. Particularly in the short period from 25 June to 1 July, where the sea-ice surface mostly consists of bare ice and melt ponds in HNnew and snow in HNold, the difference in Q_{res} between HNnew and HNold amounts on average to 45 W m^{-2}.

The effect of this amplified two-stage snow-albedo/ice-albedo feedback is demonstrated in Fig. 3 by the differences between HNold and HNnew with respect to the evolution of the Arctic sea-ice volume and extent. HNnew shows additional loss of sea-ice volume of more than 1000 km^3 during the two periods of high solar irradiance. This additional loss of sea-ice volume is not fully compensated during the subsequent freezing periods with the result that the sea-ice volume gradually decreases over the years, presumably towards a new equilibrium with mostly thinner ice. In combination with the additional loss of sea-ice volume, HNnew shows additional reduction of summer sea-ice extent of around 250,000 km^2 during the first melting period and even around 500,000 km^2 during the second melting period. In contrast to the sea-ice volume, the sea-ice extent recovers almost completely during the cold season, but the sea-ice cover becomes vulnerable for amplified reductions in subsequent melting periods due to the thinner ice.

https://doi.org/10.5194/egusphere-2023-634
Preprint. Discussion started: 11 April 2023

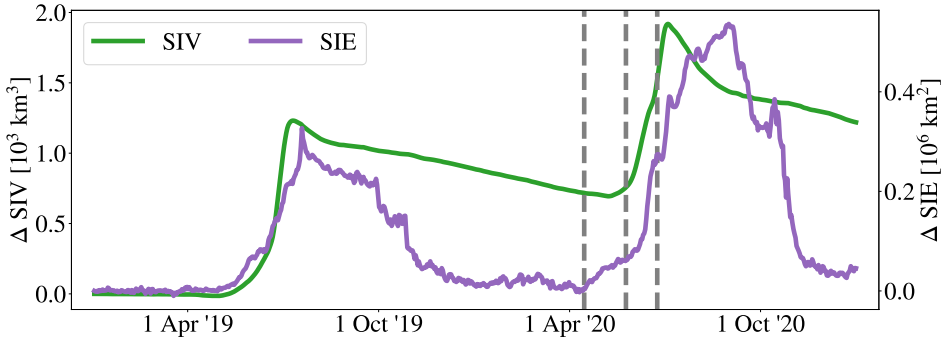

Figure 3. Time series of difference in daily mean Arctic sea-ice volume (SIV) and daily mean Arctic sea-ice extent (SIE) between HNold and HNnew for the entire simulation period 2019–2020. The dashed vertical lines indicate the albedo evaluation periods described in the context of Fig. 1.

4 Conclusions

Given that overcast conditions appear more often than cloud-free/broken-cloud conditions, one could assume that the effect of the higher albedo for overcast conditions in HNnew compared to the cloud-independent albedo in HNold overcompensates the effect of the lower albedo for cloud-free/broken-cloud conditions. Actually, the mean albedo of the entire evaluation period from 15 April 2020 to 24 June 2020 is almost equal in HNnew and HNold, which basically results from higher albedo values during the cold period and lower ones during the snow melt period in HNnew.

As the higher albedo during the cold period can be considered as entirely irrelevant for melting of snow or sea ice, the albedo differences between model simulation and observation during this period do not play an important role in the overall performance of the revised snow albedo parameterization. There are also indications that the observed surface albedo variations are not merely a result of the cloud cover, but rather dependent on the liquid water content of the clouds. Also changing surface characteristics might play a role, for instance due to snow metamorphosis or snow drift.

In contrast to the cold period, the lower albedo during the warmer period, where the snow becomes wet and starts to melt, is important. The cloud dependence in combination with the temperature dependence of the albedo appears to be sufficient in order to reproduce the observed albedo variations from a statistical point of view. In this view, the revised snow albedo parameterization represents a major improvement compared to the cloud-independent original snow albedo parameterization. In particular, the intermittently occurring lower albedo values under cloud-free/broken-cloud conditions lead to an increased heat supply at the snow surface that promotes the melting of snow. The implication in the coupled model systems is an earlier disappearance of the snow cover and an earlier onset of sea-ice melt, which translates into an amplification of the two-stage snow-albedo/ice-albedo feedback with finally profound changes in sea-ice volume and summer sea-ice extent.

The ice-albedo feedback is of course also influenced by the albedo of both bare ice and melt ponds. Also the parameterization of the respective fractions of snow, bare ice, and melt ponds are a matter of importance for a realistic simulation of the snow-albedo/ice-albedo feedback. All these aspects have been left aside in this study. Nevertheless, the significant impact on the

https://doi.org/10.5194/egusphere-2023-634
Preprint. Discussion started: 11 April 2023

simulated sea-ice volume and extent due to a rather minor modification of the snow albedo parameterization indicates how important it is to develop more realistic albedo parameterizations on the basis of observations, especially for coupled model systems.

Data availability. HIRHAM–NAOSIM data are available at the tape archive of the German Climate Computing Center (DKRZ; https://www.dkrz.de/en/systems/datenarchiv); one needs to register at DKRZ to get a user account. We will also make subsets of the data available via Swift (https://www.dkrz.de/up/systems/swift) on request. Measurements from Met City and from the Atmospheric Surface Flux Stations will soon be available at the Arctic Data Center (https://arcticdata.io/catalog/view/doi:10.18739/A2PV6B83F for Met City; https://arcticdata.io/catalog/view/doi:10.18739/A2FF3M18K for ASFS30; https://arcticdata.io/catalog/view/doi:10.18739/A2XD0R00S for ASFS50). The ShupeTurner cloud microphysics product is available at the ARM Archive (Shupe et al., 2022). The OLCI raw data are available from https://ladsweb.modaps.eosdis.nasa.gov/archive/allData/450/ and the processed MPD albedo product is available from https://data.seaice.uni-bremen.de/databrowser/#p=MERIS_OLCI_albedo.

Author contributions. All authors contributed to conception and design of the study. WD performed the model simulations. HN processed the surface albedo from the satellite data. LF conducted all other data processing, produced the figures, and analysed the results. WD wrote the first draft of the manuscript based on the insights from all co-authors. All authors contributed to manuscript revision, read, and approved the submitted version.

Competing interests. The authors declare that no competing interests are present.

Acknowledgements. WD, AR, EJ, and HN acknowledge the funding by the Deutsche Forschungsgemeinschaft (DFG, German Research Foundation) project 268020496 TRR 172, within the Transregional Collaborative Research Center "ArctiC Amplification: Climate Relevant Atmospheric and SurfaCe Processes, and Feedback Mechanisms (AC)^3". WD and AR acknowledge the funding by the European Union's Horizon 2020 research and innovation framework programme under Grant agreement no. 101003590 (PolarRES project). This work used resources of the Deutsches Klimarechenzentrum (DKRZ) under project ID aa0049. Some of the data used in this manuscript were produced as part of the international Multidisciplinary drifting Observatory for the Study of Arctic Climate (MOSAiC) with the tag MOSAiC20192020 and the project ID AWI_PS122_00. Data from autonomous atmospheric surface flux stations were provided by the University of Colorado / NOAA surface flux team. Radiation data from Met City were collected by the Atmospheric Radiation Measurement (ARM) User Facility, a DOE Office of Science User Facility managed by the Biological and Environmental Research Program. We thank all those who contributed to MOSAiC and made this endeavor possible (Nixdorf et al., 2021). We also acknowledge support by the Open Access Publication Funds of the Alfred-Wegener-Institut, Helmholtz-Zentrum für Polar- und Meeresforschung. Finally, we thank Manfred Wendisch and Matthew Shupe for their helpful comments on an earlier draft of this paper.

https://doi.org/10.5194/egusphere-2023-634
Preprint. Discussion started: 11 April 2023

References

Boucher, O., Servonnat, J., Albright, A. L., Aumont, O., Balkanski, Y., Bastrikov, V., Bekki, S., Bonnet, R., Bony, S., Bopp, L., Braconnot, P., Brockmann, P., Cadule, P., Caubel, A., Cheruy, F., Codron, F., Cozic, A., Cugnet, D., D'Andrea, F., Davini, P., de Lavergne, C., Denvil, S., Deshayes, J., Devilliers, M., Ducharne, A., Dufresne, J., Dupont, E., Éthé, C., Fairhead, L., Falletti, L., Flavoni, S., Foujols, M., Gardoll, S., Gastineau, G., Ghattas, J., Grandpeix, J., Guenet, B., Guez, L. E., Guilyardi, E., Guimberteau, M., Hauglustaine, D., Hourdin, F., Idelkadi, A., Joussaume, S., Kageyama, M., Khodri, M., Krinner, G., Lebas, N., Levavasseur, G., Lévy, C., Li, L., Lott, F., Lurton, T., Luyssaert, S., Madec, G., Madeleine, J., Maignan, F., Marchand, M., Marti, O., Mellul, L., Meurdesoif, Y., Mignot, J., Musat, I., Ottlé, C., Peylin, P., Planton, Y., Polcher, J., Rio, C., Rochetin, N., Rousset, C., Sepulchre, P., Sima, A., Swingedouw, D., Thiéblemont, R., Traore, A. K., Vancoppenolle, M., Vial, J., Vialard, J., Viovy, N., and Vuichard, N.: Presentation and evaluation of the IPSL-CM6A-LR climate model, J. Adv. Model. Earth Syst., 12, e2019MS002010, https://doi.org/10.1029/2019MS002010, 2020.

Cox, C. J., Gallagher, M., Shupe, M. D., Persson, P. O. G., Solomon, A., Fairall, C. W., Ayers, T., Blomquist, B., Brooks, I. M., Costa, D., Grachev, A., Gottas, D., Hutchings, J. K., Kutchenreiter, M., Leach, J., Morris, S. M., Morris, V., Osborn, J., Pezoa, S., Preusser, A., Riihimaki, L., and Uttal, T.: Continuous observations of the surface energy budget and meteorology over the Arctic sea ice during MOSAiC, Sci. Data, submitted, 2023.

Dorn, W., Dethloff, K., and Rinke, A.: Improved simulation of feedbacks between atmosphere and sea ice over the Arctic Ocean in a coupled regional climate model, Ocean Model., 29, 103–114, https://doi.org/10.1016/j.ocemod.2009.03.010, 2009.

Dorn, W., Rinke, A., Köberle, C., Dethloff, K., and Gerdes, R.: Evaluation of the sea-ice simulation in the upgraded version of the coupled regional atmosphere-ocean-sea ice model HIRHAM–NAOSIM 2.0, Atmosphere, 10, 431, https://doi.org/10.3390/atmos10080431, 2019.

Döscher, R., Acosta, M., Alessandri, A., Anthoni, P., Arsouze, T., Bergman, T., Bernardello, R., Boussetta, S., Caron, L.-P., Carver, G., Castrillo, M., Catalano, F., Cvijanovic, I., Davini, P., Dekker, E., Doblas-Reyes, F. J., Docquier, D., Echevarria, P., Fladrich, U., Fuentes-Franco, R., Gröger, M., v. Hardenberg, J., Hieronymus, J., Karami, M. P., Keskinen, J.-P., Koenigk, T., Makkonen, R., Massonnet, F., Ménégoz, M., Miller, P. A., Moreno-Chamarro, E., Nieradzik, L., van Noije, T., Nolan, P., O'Donnell, D., Ollinaho, P., van den Oord, G., Ortega, P., Prims, O. T., Ramos, A., Reerink, T., Rousset, C., Ruprich-Robert, Y., Sager, P. L., Schmith, T., Schrödner, R., Serva, F., Sicardi, V., Madsen, M. S., Smith, B., Tian, T., Tourigny, E., Uotila, P., Vancoppenolle, M., Wang, S., Wårlind, D., Willén, U., Wyser, K., Yang, S., Yepes-Arbós, X., and Zhang, Q.: The EC-Earth3 Earth system model for the Coupled Model Intercomparison Project 6, Geosci. Model Dev., 15, 2973–3020, https://doi.org/10.5194/gmd-15-2973-2022, 2022.

Flato, G., Marotzke, J., Abiodun, B., Braconnot, P., Chou, S. C., Collins, W., Cox, P., Driouech, F., Emori, S., Eyring, V., Forest, C., Gleckler, P., Guilyardi, E., Jakob, C., Kattsov, V., Reason, C., and Rummukainen, M.: Evaluation of Climate Models, in: Climate Change 2013: The Physical Science Basis. Contribution of Working Group I to the Fifth Assessment Report of the Intergovernmental Panel on Climate Change, edited by Stocker, T. F., Qin, D., Plattner, G.-K., Tignor, M., Allen, S. K., Boschung, J., Nauels, A., Xia, Y., Bex, V., and Midgley, P. M., chap. 9, pp. 741–866, Cambridge University Press, Cambridge, United Kingdom and New York, NY, USA, https://doi.org/10.1017/cbo9781107415324.020, 2013.

Gardner, A. S. and Sharp, M. J.: A review of snow and ice albedo and the development of a new physically based broadband albedo parameterization, J. Geophys. Res., 115, F01009, https://doi.org/10.1029/2009JF001444, 2010.

Grenfell, T. C. and Perovich, D. K.: Incident spectral irradiance in the Arctic Basin during the summer and fall, J. Geophys. Res., 113, D12117, https://doi.org/10.1029/2007JD009418, 2008.

https://doi.org/10.5194/egusphere-2023-634
Preprint. Discussion started: 11 April 2023

Hahn, L. C., Armour, K. C., Zelinka, M. D., Bitz, C. M., and Donohoe, A.: Contributions to polar amplification in CMIP5 and CMIP6 models, Front. Earth Sci., 9, 710036, https://doi.org/10.3389/feart.2021.710036, 2021.

Hersbach, H., Bell, B., Berrisford, P., Hirahara, S., Horányi, A., Muñoz-Sabater, J., Nicolas, J., Peubey, C., Radu, R., Schepers, D., Simmons, A., Soci, C., Abdalla, S., Abellan, X., Balsamo, G., Bechtold, P., Biavati, G., Bidlot, J., Bonavita, M., Chiara, G. D., Dahlgren, P., Dee, D., Diamantakis, M., Dragani, R., Flemming, J., Forbes, R., Fuentes, M., Geer, A., Haimberger, L., Healy, S., Hogan, R. J., Hólm, E., Janisková, M., Keeley, S., Laloyaux, P., Lopez, P., Lupu, C., Radnoti, G., de Rosnay, P., Rozum, I., Vamborg, F., Villaume, S., and Thépaut, J.-N.: The ERA5 global reanalysis, Q. J. R. Meteorol. Soc., 146, 1999–2049, https://doi.org/10.1002/qj.3803, 2020.

Istomina, L., Heygster, G., Huntemann, M., Marks, H., Melsheimer, C., Zege, E., Malinka, A., Prikhach, A., and Katsev, I.: Melt pond fraction and spectral sea ice albedo retrieval from MERIS data – Part 2: Case studies and trends of sea ice albedo and melt ponds in the Arctic for years 2002–2011, Cryosphere, 9, 1567–1578, https://doi.org/10.5194/tc-9-1567-2015, 2015a.

Istomina, L., Heygster, G., Huntemann, M., Schwarz, P., Birnbaum, G., Scharien, R., Polashenski, C., Perovich, D., Zege, E., Malinka, A., Prikhach, A., and Katsev, I.: Melt pond fraction and spectral sea ice albedo retrieval from MERIS data – Part 1: Validation against in situ, aerial, and ship cruise data, Cryosphere, 9, 1551–1566, https://doi.org/10.5194/tc-9-1551-2015, 2015b.

Jäkel, E., Stapf, J., Wendisch, M., Nicolaus, M., Dorn, W., and Rinke, A.: Validation of the sea ice surface albedo scheme of the regional climate model HIRHAM–NAOSIM using aircraft measurements during the ACLOUD/PASCAL campaigns, Cryosphere, 13, 1695–1708, https://doi.org/10.5194/tc-13-1695-2019, 2019.

Klaus, D., Dethloff, K., Dorn, W., Rinke, A., and Wu, D. L.: New insight of Arctic cloud parameterization from regional climate model simulations, satellite-based, and drifting station data, Geophys. Res. Lett., 43, 5450–5459, https://doi.org/10.1002/2015GL067530, 2016.

Køltzow, M.: The effect of a new snow and sea ice albedo scheme on regional climate model simulations, J. Geophys. Res., 112, D07110, https://doi.org/10.1029/2006JD007693, 2007.

Light, B., Smith, M. M., Perovich, D. K., Webster, M. A., Holland, M. M., Linhardt, F., Raphael, I. A., Clemens-Sewall, D., Macfarlane, A. R., Anhaus, P., and Bailey, D. A.: Arctic sea ice albedo: Spectral composition, spatial heterogeneity, and temporal evolution observed during the MOSAiC drift, Elem. Sci. Anth., 10, 000103, https://doi.org/10.1525/elementa.2021.000103, 2022.

Liu, J., Zhang, Z., Inoue, J., and Horton, R. M.: Evaluation of snow/ice albedo parameterizations and their impacts on sea ice simulations, Int. J. Climatol., 27, 81–91, https://doi.org/10.1002/joc.1373, 2007.

Nixdorf, U., Dethloff, K., Rex, M., Shupe, M., Sommerfeld, A., Perovich, D. K., Nicolaus, M., Heuzé, C., Rabe, B., Loose, B., Damm, E., Gradinger, R., Fong, A., Maslowski, W., Rinke, A., Kwok, R., Spreen, G., Wendisch, M., Herber, A., Hirsekorn, M., Mohaupt, V., Frickenhaus, S., Immerz, A., Weiss-Tuider, K., König, B., Mengedoht, D., Regnery, J., Gerchow, P., Ransby, D., Krumpen, T., Morgenstern, A., Haas, C., Kanzow, T., Rack, F. R., Saitzev, V., Sokolov, V., Makarov, A., Schwarze, S., Wunderlich, T., Wurr, K., and Boetius, A.: MOSAiC Extended Acknowledgement, Zenodo, https://doi.org/10.5281/zenodo.5541624, 2021.

Pithan, F. and Mauritsen, T.: Arctic amplification dominated by temperature feedbacks in contemporary climate models, Nat. Geosci., 7, 181–184, https://doi.org/10.1038/NGEO2071, 2014.

Pohl, C., Istomina, L., Tietsche, S., Jäkel, E., Stapf, J., Spreen, G., and Heygster, G.: Broadband albedo of Arctic sea ice from MERIS optical data, Cryosphere, 14, 165–182, https://doi.org/10.5194/tc-14-165-2020, 2020.

Shine, K. P. and Henderson-Sellers, A.: The sensitivity of a thermodynamic sea ice model to changes in surface albedo parameterization, J. Geophys. Res., 90, 2243–2250, https://doi.org/10.1029/JD090iD01p02243, 1985.

Shupe, M. D.: ShupeTurner cloud microphysics product, ARM Mobile Facility (MOS) MOSAiC (Drifting Obs – Study of Arctic Climate), https://doi.org/10.5439/1871015, 2022.

https://doi.org/10.5194/egusphere-2023-634
Preprint. Discussion started: 11 April 2023

Shupe, M. D., Rex, M., Blomquist, B., Persson, P. O. G., Schmale, J., Uttal, T., Althausen, D., Angot, H., Archer, S., Bariteau, L., Beck, I., Bilberry, J., Bucci, S., Buck, C., Boyer, M., Brasseur, Z., Brooks, I. M., Calmer, R., Cassano, J., Castro, V., Chu, D., Costa, D., Cox, C. J., Creamean, J., Crewell, S., Dahlke, S., Damm, E., de Boer, G., Deckelmann, H., Dethloff, K., Dütsch, M., Ebell, K., Ehrlich, A., Ellis, J., Engelmann, R., Fong, A. A., Frey, M. M., Gallagher, M. R., Ganzeveld, L., Gradinger, R., Graeser, J., Greenamyer, V., Griesche, H., Griffiths, S., Hamilton, J., Heinemann, G., Helmig, D., Herber, A., Heuzé, C., Hofer, J., Houchens, T., Howard, D., Inoue, J., Jacobi, H.-W., Jaiser, R., Jokinen, T., Jourdan, O., Jozef, G., King, W., Kirchgaessner, A., Klingebiel, M., Krassovski, M., Krumpen, T., Lampert, A., Landing, W., Laurila, T., Lawrence, D., Lonardi, M., Loose, B., Lüpkes, C., Maahn, M., Macke, A., Maslowski, W., Marsay, C., Maturilli, M., Mech, M., Morris, S., Moser, M., Nicolaus, M., Ortega, P., Osborn, J., Pätzold, F., Perovich, D. K., Petäjä, T., Pilz, C., Pirazzini, R., Posman, K., Powers, H., Pratt, K. A., Preußer, A., Quéléver, L., Radenz, M., Rabe, B., Rinke, A., Sachs, T., Schulz, A., Siebert, H., Silva, T., Solomon, A., Sommerfeld, A., Spreen, G., Stephens, M., Stohl, A., Svensson, G., Uin, J., Viegas, J., Voigt, C., von der Gathen, P., Wehner, B., Welker, J. M., Wendisch, M., Werner, M., Xie, Z., and Yue, F.: Overview of the MOSAiC expedition: Atmosphere, Elem. Sci. Anth., 10, 00060, https://doi.org/10.1525/elementa.2021.00060, 2022.

Stapf, J., Ehrlich, A., Jäkel, E., Lüpkes, C., and Wendisch, M.: Reassessment of shortwave surface cloud radiative forcing in the Arctic: consideration of surface-albedo–cloud interactions, Atmos. Chem. Phys., 20, 9895–9914, https://doi.org/10.5194/acp-20-9895-2020, 2020.

Toyoda, T., Aoki, T., Niwano, M., Tanikawa, T., Urakawa, L. S., Tsujino, H., Nakano, H., Sakamoto, K., Hirose, N., and Yamanaka, G.: Impact of observation-based snow albedo parameterization on global ocean simulation results, Polar Sci., 24, 100521, https://doi.org/10.1016/j.polar.2020.100521, 2020.

Warren, S. G.: Optical properties of snow, Rev. Geophys., 20, 67–89, https://doi.org/10.1029/RG020i001p00067, 1982.

Zege, E., Malinka, A., Katsev, I., Prikhach, A., Heygster, G., Istomina, L., Birnbaum, G., and Schwarz, P.: Algorithm to retrieve the melt pond fraction and the spectral albedo of Arctic summer ice from satellite optical data, Remote Sens. Environ., 163, 153–164, https://doi.org/10.1016/j.rse.2015.03.012, 2015.

Zuo, H., Balmaseda, M. A., Tietsche, S., Mogensen, K., and Mayer, M.: The ECMWF operational ensemble reanalysis–analysis system for ocean and sea ice: a description of the system and assessment, Ocean Sci., 15, 779–808, https://doi.org/10.5194/os-15-779-2019, 2019.